RSC Advances

PAPER



Cite this: *RSC Adv.*, 2024, **14**, 3122

# Novel porphyrin derivative containing cations as new photodynamic antimicrobial agent with high efficiency†

Jiajing Zhang, ‡[abc] Xiaoqian Yuan, ‡[c] Hongsen Li,[c] Liting Yu,[c] Yulong Zhang,[c] Keyi Pang,[c] Chaoyue Sun,[c] Zhongyang Liu,[c] Jie Li,[c] Liying Ma,*[c] Jinming Song[ad] and Lingxin Chen *[bc]

Bacterial infections from chronic wounds affect about 175 million people each year and are a significant clinical problem. Through the integration of photodynamic therapy (PDT) and chemotherapy, a new photosensitizer consisting of ammonium salt *N*,*N*-bis-(2-hydroxyethyl)-*N*-(6-(4-(10,15,20-trimesitylporphyrin-5-yl) phenoxy) hexane)-*N*-methanaminium bromide, $TMP^{(+)}$ was successfully synthesized with a total reaction yield of 10%. The novel photosensitizer consists of two parts, a porphyrin photosensitizer part and a quaternary ammonium salt part, to achieve the synergistic effect of photodynamic and chemical antibacterial activity. With the increase of $TMP^{(+)}$ concentration, the diameter of the PCT fiber membranes (POL/COL/$TMP^{(+)}$; POL, polycaprolactone; COL, collagen) gradually increased, which was caused by the charge of the quaternary ammonium salt. At the same time, the antibacterial properties were gradually improved. We finally selected the PCT 0.5% group for the antibacterial experiment, with excellent performance in fiber uniformity, hydrophobicity and biosafety. The antibacterial experiment showed that the modified porphyrin $TMP^{(+)}$ had a better antibacterial effect than others. *In vivo* chronic wound healing experiments proved that the antibacterial and anti-inflammatory effect of the PCTL group was the best, further confirmed by H&E histological analysis, immunofluorescence and immunohistochemistry mechanism experiments. This research lays the foundation for the manufacture of novel molecules that combine chemical and photodynamic strategies.

Received 13th November 2023
Accepted 8th January 2024

DOI: 10.1039/d3ra07743h

rsc.li/rsc-advances

## Introduction

Open skin wounds resulting from cuts, burns, and surgical incisions are vulnerable to infection from pathogens and microorganisms present in the surrounding environment, mucous membranes, and adjacent skin.[1,2] This may lead to serious complications and chronic wounds, which present a significant threat to public health. According to WHO statistics, about 175 million people are affected by infection every year, and *E. coli* (17.2%) and *S. aureus* (15.2%) are the two most common bacteria for causing wound infection.[2] To solve this problem, a series of antibacterial wound dressings, including antibiotics,[3] metal ions ($Ag^+$)[4,5] and quaternary ammonium cations (QACs),[6,7] have been extensively studied. Antibiotics are the most common treatments used to prevent wound infections. Nonetheless, routine antibiotic therapy results in bacterial resistance and environmental pollution, presenting a challenge in the treatment of wound infections.[8] On the other hand, prolonged exposure to $Ag^+$ may lead to skin discoloration (argyria) or even Ag-resistant bacteria, limiting the effectiveness of this treatment approach.[4,5] Moreover, QACs are cytotoxic to normal cells and are prone to inactivation under alkaline conditions of infected wounds.[6,7] More importantly, the above antibacterial wound dressings often possess only a single antibacterial function, which usually necessitates a higher concentration of the antibacterial substance; the latter may potentially lead to environmental and safety concerns. Therefore, there is an urgent need for new strategies to develop novel wound dressings with antibacterial properties that are not only

[a]*CAS Key Laboratory of Marine Ecology and Environmental Sciences, Institute of Oceanology, Chinese Academy of Sciences, Qingdao 266071, China. E-mail: jiajing_z@bzmc.edu.cn; jmsong@qdio.ac.cn*

[b]*CAS Key Laboratory of Coastal Environmental Processes and Ecological Remediation, Yantai Institute of Coastal Zone Research, Chinese Academy of Sciences, Yantai 264003, China. E-mail: lxchen@yic.ac.cn*

[c]*School of Pharmacy, Binzhou Medical University, Yantai 264003, China. E-mail: y17865581988@163.com; BZlhs714@163.com; yult1992@163.com; yulongzhang2019@163.com; 19712051585@163.com; 19712051380@163.com; lzy15069001356@163.com; 13361194986@163.com*

[d]*Laboratory for Marine Biology and Biotechnology, Pilot National Laboratory for Marine Science and Technology, Qingdao 266237, China*

† Electronic supplementary information (ESI) available: Fig. S1, Table S1 and Video S1. See DOI: https://doi.org/10.1039/d3ra07743h

‡ These authors contributed equally to this work.

highly effective, but also eco-friendly. This will help reduce the dosage of drugs used in the treatment, mitigate antimicrobial resistance, and reduce environmental pollution.

PDT is an effective method for clinical antimicrobial therapy that employs photosensitizers (PSs) to convert molecular oxygen into highly bactericidal reactive oxygen species (ROS) upon exposure to light. Compared to other traditional treatments, PDT offers three notable advantages.[8–10] Primarily, PDT can effectively overcome drug resistance from pathogens by generating ROS that indiscriminately disrupt membrane lipids, proteins and DNA. Moreover, PDT offers the advantage of precise spatial and temporal control, thereby reducing the potential side effects on healthy cells and tissues. Thirdly, PDT can achieve low-dose drug loading and recycling, when stable, non-consumable photosensitizers are used. Despite these advancements, it is imperative to enhance the antibacterial activity of PSs. In biological systems, the generated highly reactive $^1O_2$ usually has a high decay rate with a half-life of less than 0.4 μs, resulting in a short diffusion distance of less than 0.02 μm.[11,12] To enhance the photo-bactericidal activity, photosensitizers (PSs), such as porphyrin species, have been recently synthesized or assembled into antibacterial materials, such as by electrospinning, to ensure the produced $^1O_2$ displays effective cytotoxic activity at the required distance at the infected sites.[13,14] This will ensure that the generated $^1O_2$ exerts potent cytotoxicity at the required distance from the site of infection. Besides, the incorporation of dual bactericidal mechanisms including PDT and chemotherapy on the same molecular platform, would be a great strategy to address resistance while enhancing bactericidal activity.

In recent years, there has been extensive exploration of cationic porphyrins in photobiological inactivation of Gram(+) and Gram(−) bacteria.[15–25] Most of the work focuses on the research of antibacterial materials based on a porphyrin-based self-assembly system.[15,21–25] There are few researches on the direct modification of porphyrins as the parent.[16–19] However, due to the π–π interaction of planar large conjugated porphyrin rings, porphyrins and their derivatives are prone to be self-quenching, which reduces the production of $^1O_2$ and the efficiency of photodynamic antibacterial.[19–25] To address the challenge of the π–π interaction of the planar large conjugate porphyrin rings, quaternary ammonium salt cationic groups with antibacterial properties were designed to inhibit π–π interaction through electrostatic repulsion, enhance the generation of $^1O_2$, improve the efficiency of photodynamic therapy, and achieve synergistic antibacterial effect through the combination of QAC-based chemotherapy and phototherapy.[14,24–26] More importantly, cations tend to selectively attach to negatively charged microbial cells rather than electrically neutral mammalian cells, effectively reducing cytotoxic effects on healthy tissues.[27]

In this work, we synthesized a new porphyrin derivative $TMP^{(+)}$ molecule, consisting of a quaternary ammonium salt part and a porphyrin photosensitizer part. A series of nanofiber films including PC (POL/COL, nanofiber membranes with only POL and COL), PCT with different photosensitizer concentrations (0.02%, 0.05%, 0.1%, 0.2% and 0.5%) were obtained by electrospinning POL, COL and $TMP^{(+)}$. *In vitro* biological experiments showed that PCT membranes had low toxicity, good biocompatibility and high antibacterial activity. ROS detection showed that PCT membranes had high $^1O_2$ production efficiency and the recycling experiment showed that PCT membranes could be recycled more than 10 times, demonstrating their suitability as photodynamic antibacterial materials. *In vivo* antibacterial experiments showed that the PCTL (PCT 0.5% with light) group showed promising bactericidal properties, while simultaneously accelerating the healing of the back wound model of *Staphylococcus aureus* infected mice; the mechanism of inflammation reduction was also verified. Through the combination of chemotherapy and phototherapy, the concentration of traditional antibacterial drugs is reduced, thus effectively reducing their cytotoxicity. Meanwhile, the ROS bactericidal strategy can effectively prevent the generation of drug-resistant strains, providing novel opportunities for combating bacterial drug resistance (Fig. 1).

## Results and discussion

### Preparation and characterization of PC and PCT

5-(4-Hydroxyphenyl)-10,15,20-trimesitylporphyrin (TMPOH) was synthesized according to literature procedures,[28] with a $^1H$ NMR single peak of phenyl-OH at $\delta$ 5.32 ppm (see Fig. S1†). The new intermediate TMP-O$(CH_2)_6$Br was obtained by a nucleophilic substitution reaction between TMPOH with 1,6-dibromohexane. A $^1H$ NMR triplet peak ($J = 6.5$ Hz) of phenyl-O-$CH_2$ at $\delta$ 4.27 ppm (see Fig. S4†) together with a singlet of phenyl-O-$CH_2$ at $\delta$ 67.97 ppm in $^{13}C$ DEPT NMR (see Fig. S5†) unambiguously confirmed the proposed structure, which was also supported by ESI-MS (see Fig. S6†). The $^1H$ NMR signals of $NCH_2CH_2OH$ in *N*-methyldiethanolamine appear as broad single peaks ($\delta$ 3.80 ppm, 3.43 ppm, Fig. S7†). This is due to the change in relaxation time caused by the presence of anions and cations on the $TMP^{(+)}$. In Fig. S8,† the single peak of $NCH_2$-$CH_2OH$ with chemical shifts of 63.03 ppm and 62.19 ppm in $^{13}C$ DEPT NMR, together with the ESI-MS result (see Fig. S9†) confirmed the structure of $TMP^{(+)}$.

The preparation of PC and PCT nanofiber membranes was accomplished by thoroughly mixing the precursor before electrospinning. The scanning electron microscopy (SEM) images in Fig. 2A showed that with the $TMP^{(+)}$ mass fraction in nanofiber membranes increasing from 0, 0.02%, 0.05%, 0.1%, 0.2% to 0.5%, the average fiber diameter also presents an obvious increasing trend from 91 nm, 131 nm, 134 nm, 294 nm, 382 nm to 458 nm, respectively. This is due to the increased electrical conductivity of the spinning solution with the addition of $TMP^{(+)}$. To ensure a good micro–nano structure, the $TMP^{(+)}$ volume mass fraction should preferably be controlled within 0.5%. In Fig. 3A, the TGA curves showed that the first-stage weight loss was 3.35 wt%, occurring at 30–140 °C as a result of water evaporation. The most significant weight loss (~77.02 wt%) occurs in the range of 220.0–500.0 °C, related to the endothermic peaks for the decomposition of PCL and COL chains. All the dressings remain above 90.0 °C at the time of thermal decomposition (T95%), proving their good thermal

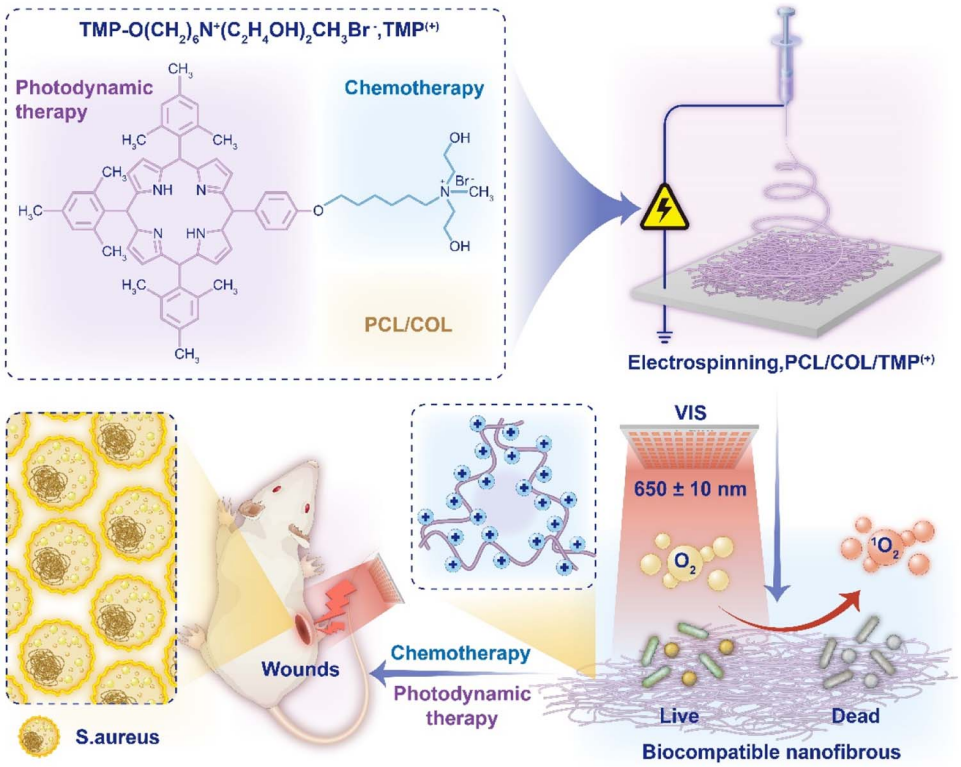


Fig. 1 Schematic illustration of the novel $TMP^{(+)}$ molecule and electrospun nanofibrous dressings PCT for accelerating infected wound healing.

stability for skin tissue engineering. Since the contact angles of all membranes were less than 90° (Fig. 3B and C), the dressings still exhibited hydrophilicity to provide a good microenvironment for wound healing.

### Biocompatibility

The Cell Counting Kit-8 (CCK-8) was employed to test for cytotoxicity in the L929 cell line (Fig. S13†).[29] The cells were incubated in the dark at 37 °C for 24 h and then examined. Results showed that all nanofiber membranes had cell viability above 100%, indicating that there were no adverse effects on mammalian cells. To eliminate the environmental influence, 3 h under natural light (at room temperature, 0.04 ± 0.02 mW $cm^{-2}$) was set as the control group. Owing to the massive production of ROS under 3 h irradiation, as the concentration of drug $TMP^{(+)}$ increased, the cell survival rates of all the PCT groups gradually decreased, but remained higher than 75%. This result not only confirmed that PCT showed low cytotoxicity, but also verified that irradiation and higher concentration $TMP^{(+)}$ promoted ROS production, as inferred from the decrease in cell viability. Therefore, the following *in vitro* and *in vivo* experiments were carried out with the PCT 0.5% membrane. In subsequent analysis, hemolysis was conducted to assess the blood compatibility of biomaterials (Fig. S14†), which found that the hemolysis rates of PC, PCT 0.02%, PCT 0.05%, PCT 0.1%, PCT 0.2%, and PCT 0.5% were 0.34 ± 0.11%, 0.38 ± 0.06%, 0.58 ± 0.37%, 0.66 ± 0.23%, 0.74 ± 0.11%, and 1.2 ± 0.14%, respectively, compared to the control group. In the above experiments, the average hemolysis rate for PCT is less than 5%, indicating that it could not cause hemolysis and meet the clinical blood safety requirements.

### Measurement of singlet oxygen ($^1O_2$)

The production of the highly reactive singlet oxygen species is essential for photodynamic therapy. The quantities of ROS generated from different PCT membranes under light exposure in natural light indoors and at room temperature were quantified using 1,3-diphenylisobenzofuran (DPBF) as a chemical sensing agent.[30] The detection mechanism is based on the fact that the generated $^1O_2$ can irreversibly quench DPBF absorbance at 410 nm upon light irradiation. As shown in Fig. 4A pure DPBF and PC film showed no change in absorbance at 410 nm after continuous irradiation for 80 min, indicating that the generation of $^1O_2$ was negligible. However, in the PCT membranes, the absorbances of DPBF at 410 nm gradually decreased with an increase in the duration of light irradiation. In addition, the PCT 0.5% group exhibited the sharpest decline in DPBF absorbance during the illumination process and then tended to stabilize the earliest because of exhausted oxygen. Fig. 4B showed that under the same irradiation conditions, when DPBF was used as a test probe, the PCT 0.5% group produced the same amount of ROS as nanofiber membranes PCP (POL/COL/TMPOH) prepared with 0.5% volume mass ratio of the unmodified porphyrin precursor TMPOH, indicating that the structural modification does not affect the production of ROS. The cycle experiment in Fig. 4C showed that the prepared

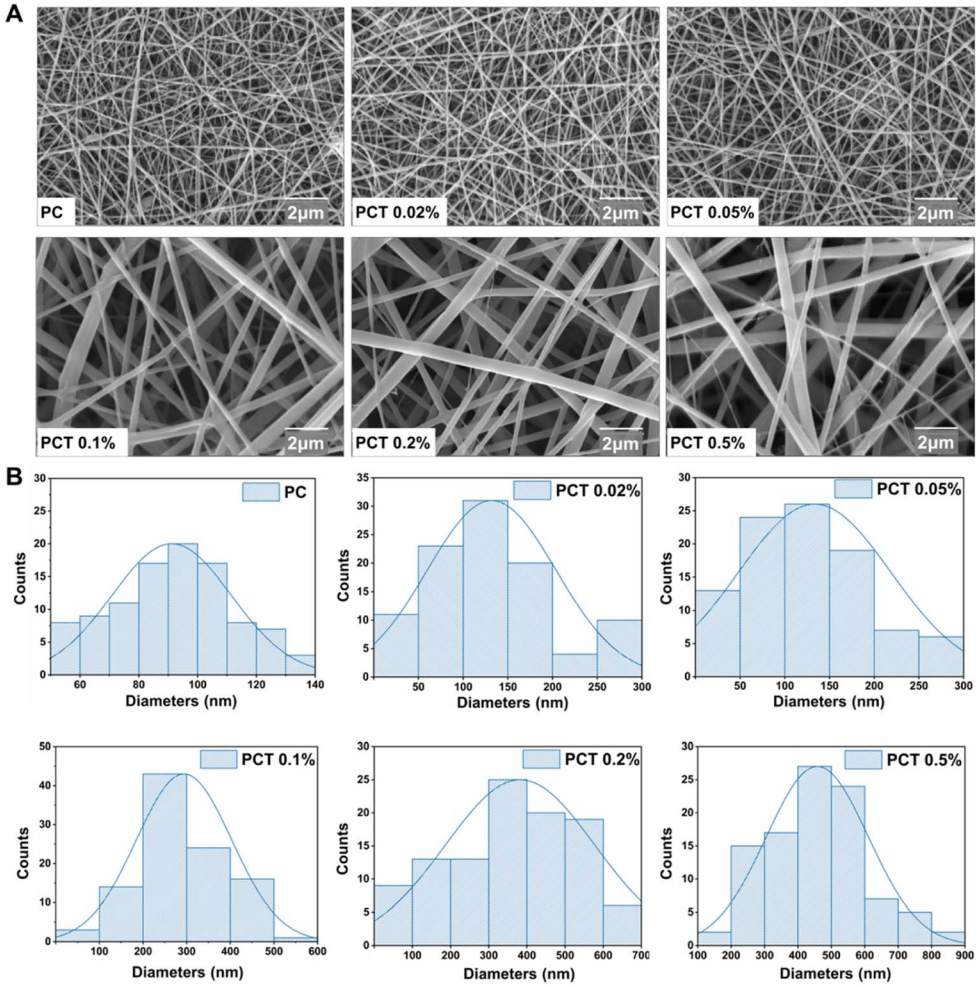


Fig. 2 (A) Representative SEM images ((a) PC, (b) PCT 0.02%, (c) PCT 0.05%, (d) PCT 0.1%, (e) PCT 0.2%, (f) PCT 0.5%). (B) Diameter distributions of corresponding PC and PCT nanofiber membranes.

PCT nanofiber membranes could effectively generate ROS production by illumination, and could be reused many times, that is, the absorbance reduction of DPBF solution remains the same after 10 cycles. Overall, the results indicated that both the presence of TMP(+) and irradiation are essential for the generation of ROS from PCT.

### *In vitro* antibacterial activity

If a bacteria-infected wound does not heal quickly, fibroblast differentiation is impaired, ultimately damaging other normal tissues in the body and the immune system. Therefore, it is crucial to develop functional materials that can not only effectively treat bacterial infections on wound surfaces but also resist bacterial drug resistance. The antibacterial activity of the synthesized membranes was qualitatively determined by monitoring the growth of residual bacteria on each membrane after photo-sterilization, measured by evaluating turbidity at 600 nm.[31–33] In this study, $G^+$ *S. aureus* and $G^-$ *E. coli* were selected as representative pathogens to evaluate the antibacterial activity of PCT with and without 650 nm light (for 3 h, 9.0 ± 0.5 mW $cm^{-2}$). We calculated the relative bacteriostatic rate of each group and the number rate of bacteria in the control group PC at 100%. According to the test results in Fig. 5A and Table S1,† the average relative $G^+$ *S. aureus* survival rates of PCT 0.02%, PCT 0.05%, PCT 0.1%, PCT 0.2%, PCT 0.5%, and PCP 0.5% were 93.94%, 76.52%, 70.08%, 63.26%, 56.44% and 96.33% in dark; and 77.53%, 50.06%, 36.74%, 34.48%, 2.85% and 13.59% under irradiation. As in Fig. 5B and Table S2† shown, the average relative $G^-$ *E. coli* survival rates of PCT 0.02%, PCT 0.05%, PCT 0.1%, PCT 0.2%, PCT 0.5% and PCP 0.5% were 78.01%, 66.91%, 57.13%, 28.73%, 25.83% and 97.82% in dark groups; 58.83%, 58.67%, 39.17%, 7.67%, 6.17% and 15.41% under irradiation. In conclusion, due to the existence of quaternary ammonium salt groups, with the increase of the concentration of $TMP^{(+)}$, the antibacterial effect was also enhanced compared to PC even without light, and the highest bactericidal rates of PCT 0.5% were 43.56% ($G^+$ *S. aureus*) and 74.17% ($G^-$ *E. coli*). Gratifyingly, the PCT 0.5% membrane showed a highly efficient antibacterial behavior (Fig. 5C and D) with 650 nm light to generate ROS, which had significant inhibitory effects on $G^+$ *S. aureus* (97.15%) and $G^-$ *E. coli* (93.83%). Compared with much previous literature, such as

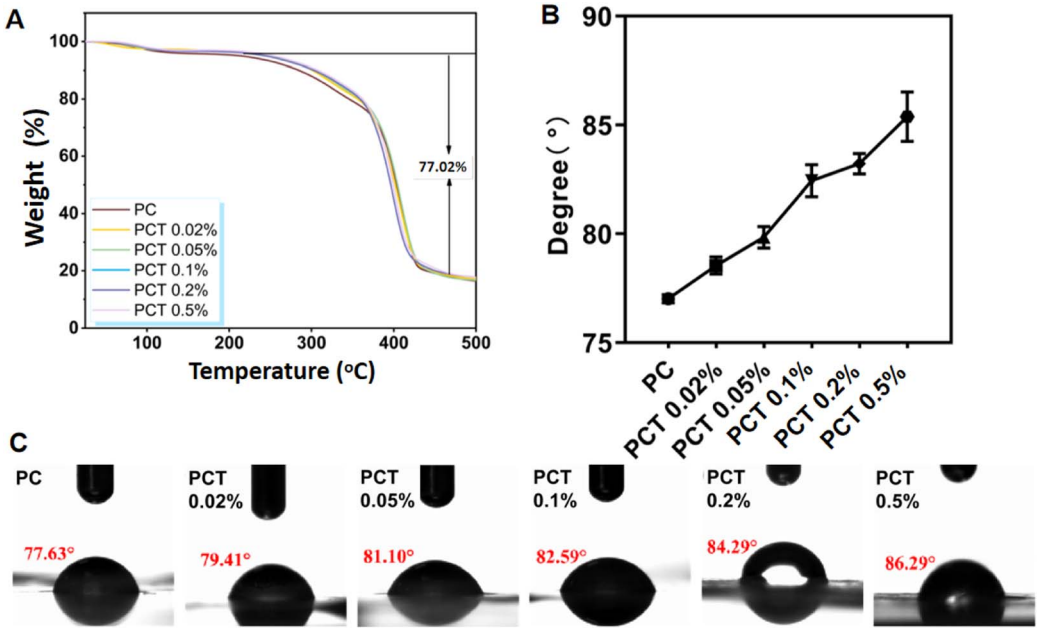


Fig. 3 (A) TGA of PC and PCT nanofiber membranes. (B) Trends of water contact angle of the PC and PCT nanofiber membranes. (C) Water contact angle measurement of composite nanofiber membrane with a matrix of PC and PCT nanofiber membranes.

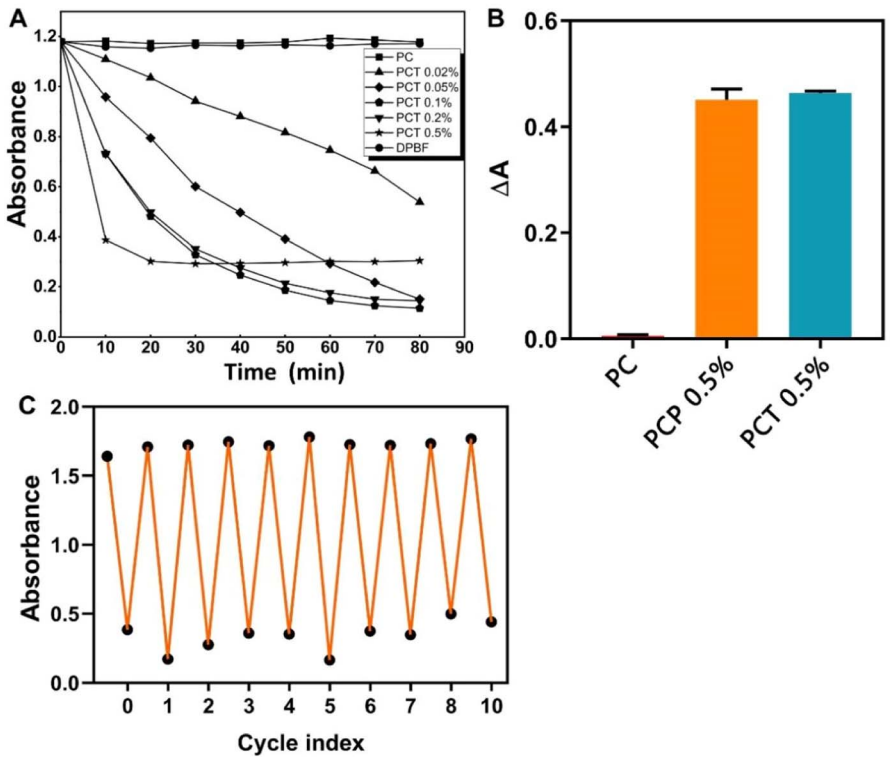


Fig. 4 (A) Absorbance curves of DPBF solution and PC, PCT membranes at different concentrations under light. (B) Comparison of absorbance changes between PC, PCP 0.5% and PCT 0.5% under light conditions. (C) Photodynamic cycling of PCT 0.5%.

nanoparticle systems, there is no lack of metal ion coordination and bactericidal effects or antibacterial drugs.[34–36] The antibacterial effect of the above systems can reach over 95%. At the same time, the presence of these auxiliary materials also has certain toxicity, so we want to achieve dual antibacterial functions within a single molecule. This result directly proved the dual antibacterial properties of the PCT, namely the chemical antibacterial effect of quaternary ammonium salt groups in the

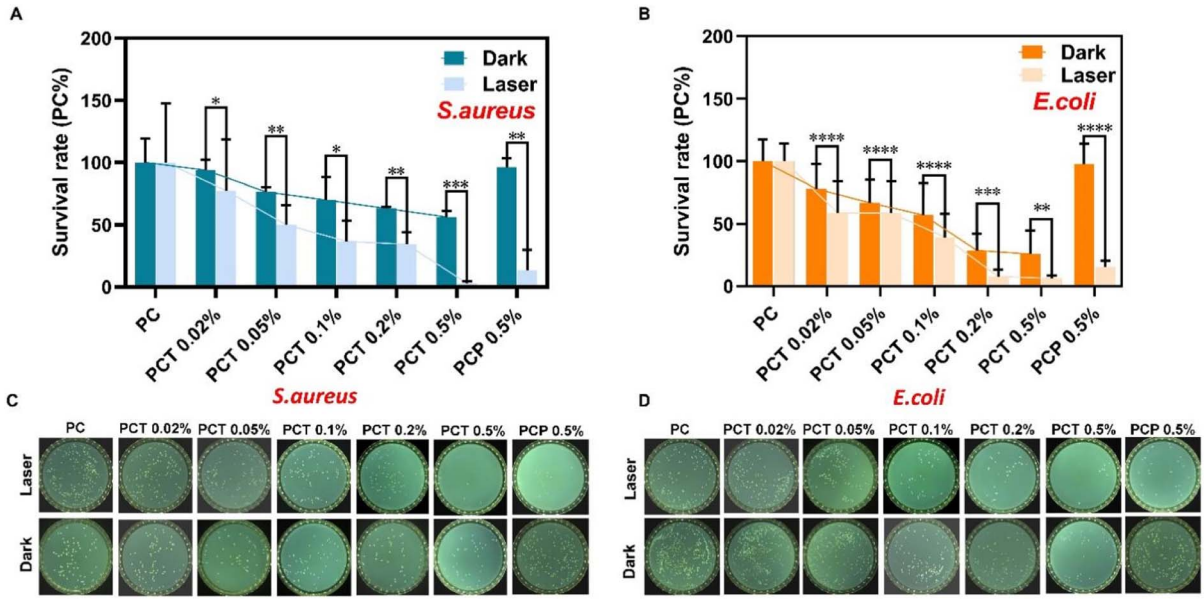


Fig. 5 Antibacterial effect of nano-fiber membrane containing TMPOH (PCP 0.5%) before modification and TMP(+) at different concentrations on *S. aureus* (A) (* for $P < 0.05$, ** for $P < 0.01$, *** for $P < 0.001$, and **** for $P < 0.0001$ and NS = no significance) and *E. coli* (B) (* for $P < 0.05$, ** for $P < 0.01$, *** for $P < 0.001$, and **** for $P < 0.0001$ and NS = no significance) under different conditions. Images of *S. aureus* (C) and *E. coli* (D) treated with nanofiber membranes containing TMPOH (PCP 0.5%) and different concentrations of TMP(+) under different conditions.

dark and the antibacterial effect of porphyrin-based singlet oxygen production *via* photosensitization. More importantly, we supposed that compared with the self-assembly system in the literature,[31–33,37] the relatively low drug concentration and high efficacy were attributed to the intermolecular electrostatic repulsion of positive charges between porphyrin molecules and electrospinning, which reduced the self-quenching effect caused by π–π stacking and thus increased ROS production.

### *In vivo* anti-infection evaluation

To investigate whether the PCT membranes can kill bacteria on the skin wound surface and thus improve wound healing, we constructed a full-thickness wound model (8 mm in diameter) on the dorsal skin of BALB/C mice which was infected with $G^+$ *S. aureus*. Subsequently, the wound healing was monitored using visual photographs which were used to determine the closure rate. Fig. 6A showed that all wounds developed different degrees of sepsis after 3 days due to bacterial infection, among which the abscess symptoms in the PCTL group (PCT 0.5% with 650 nm light) with wound healing rate of 46.84% were slightly less severe than other groups (the fitted values of Fig. 6B are: blank 14.79%, 3 M 25.11%, PC 29.12%, PCT 41.97%), which may be the result of PDT effect during the first dressing therapy. The PCTL group was treated with PDT once after observation on the 3rd day. The wound healing results on the 7th day showed that the PCTL group healed the fastest, with an 81.14% healing rate, while the healing rates of the blank group, 3 M group, PC group and PCT group were 73.64%, 74.14%, 74.43% and 76.02%, respectively. Similar to many reports in the literature, the first week after bacterial infection is usually the most significant effect of antimicrobial therapy.[38–42] The experimental results show that the single novel porphyrin cationic derivative with a double antibacterial mechanism has a definite antibacterial effect, especially under the condition of light. The results on the 10th day showed that the healing rate of the PCTL group was 94.57%, while that of the blank group, 3 M group, PC group and PCT group were 84.85%, 89.11%, 91.69% and 93.35%. On the 14th day, the PCTL group healed almost completely, while the healing rates of the blank group and 3 M group were 89.09% and 91.74%. After comprehensive analysis of the above results (Fig. 6A–C and Table S3†), the recovery of the PCT group was significantly faster than that of the blank group and 3 M group, indicating that the quaternary ammonium salt structure played a noticeable antibacterial role when no light was added. The recovery rate of the PCTL group was faster than that of the PCT group (without light), indicating that the combination of the photodynamic antibacterial strategy with the quaternary ammonium salt antibacterial strategy is very effective, and the synergistic effect of the two accelerates the repair of the full-layer skin damage caused by $G^+$ *S. aureus* infection. During the wound healing process, we monitored changes in the weight of the mice. Significant weight increases were observed in the first 7 days. This is because the wounds were inflamed and the tissue healing has increased substantially. After seven days, changes in the weight of the mice were not significant, and this was due to autoimmunity in mice (Fig. 6D). To further test its antibacterial effect, the wound tissue was investigated and the number of colony formations was counted on the 7th day after treatment. As shown in the extract of the wound specimen on the 7th day each group was coated with bacterial culture (Fig. 6E). The coating results showed that the number of bacteria in the PCTL group, PCT group, PC group and blank group decreased successively. This showed that the quaternary

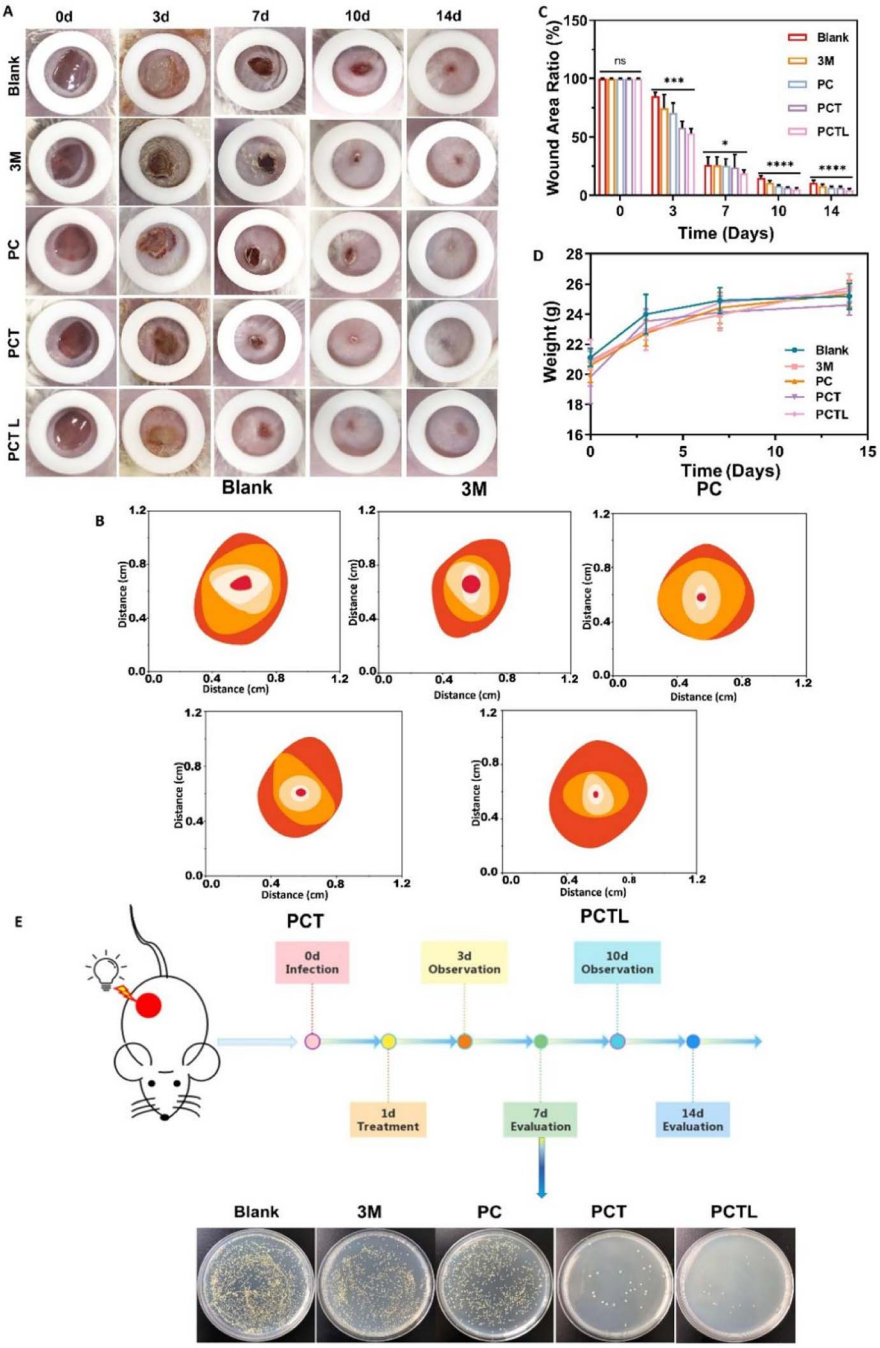


Fig. 6 (A) *In vivo* evaluation of membranes as an anti-infection wound dressing in *S. aureus*-infected mice wound model. Representative images of wounds treated with blank, PC, PCT and PCTL at different time points. (B) Schematic diagram of the wound area of the damaged skin of mice over time. (C) The wound area ratio at the indicated time points for each group. * for $P < 0.05$, ** for $P < 0.01$, *** for $P < 0.001$, and **** for $P < 0.0001$ and NS = no significance (D) the changing trend of body weight in mice during wound healing. (E) The LB-agar photographs of bacteria colonies on the 7th day were harvested from different wound tissues.

ammonium salt group had an antibacterial effect, and light could effectively enhance the antibacterial performance of the material through PDT. The above animal experiments fully prove that the new antibacterial membrane designed and synthesized by us has a strong bactericidal effect and can effectively promote the rapid healing of infected wounds. The subsequent mechanism experiment further verified its effect.

As shown in Fig. 7A, histological analysis based on hematoxylin and eosin (H&E) staining was performed on days 3, 7 and 14 to confirm the pathology of the infected wound during the healing progress. On day 3, an obvious inflammation reaction was found in blank, 3 M and PC groups due to the bacterial infection, which was reflected by blue staining *via* H&E staining. The PCT treatment partly relieved

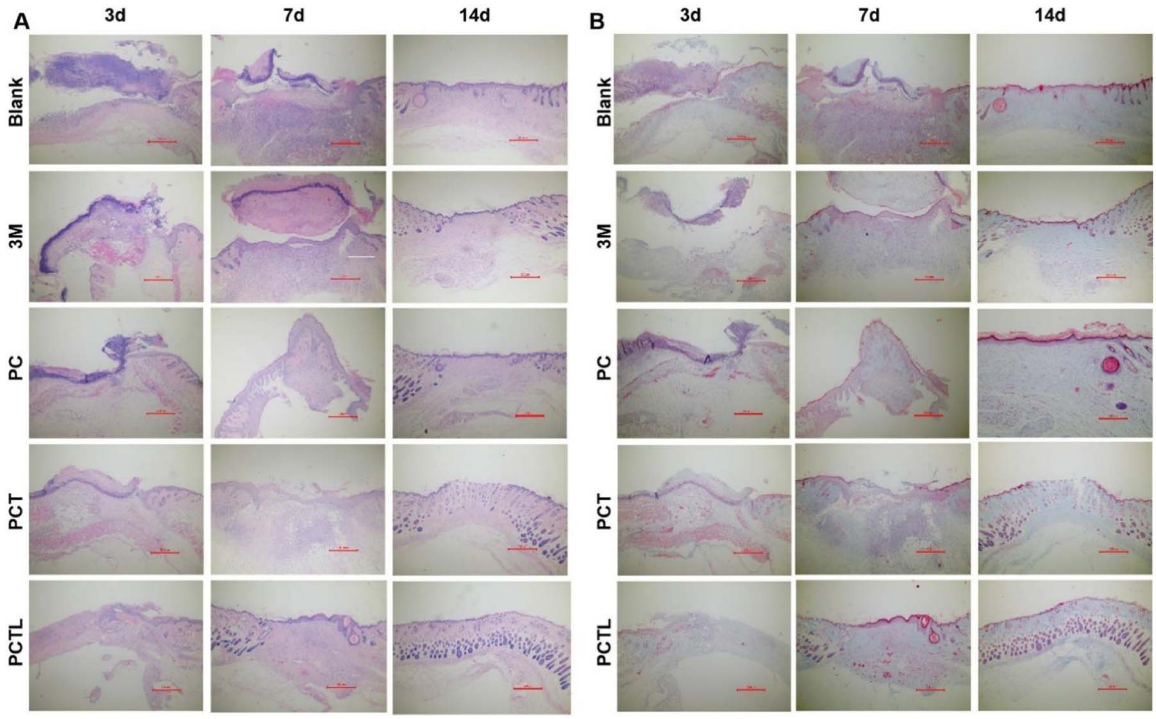


Fig. 7 (A) H&E histological analysis of the regenerated skin tissue on days 3, 7, and 14 with different treatments in *S. aureus* infected models (scale bar: 500 μm, $n = 4$ mice per group; for the meanings of the five groups, please refer to Section 3.2.13). (B) Masson's staining on the 3rd, 7th and 14th days.

inflammation, while PCTL treatment significantly inhibited the inflammation. On the 7th day after treatment, thicker epithelialized areas, more granulation tissue and neovascularization were observed in the PCTL group. On day 14, the skin tissue of the wound group treated with the PCTL group showed near-complete regeneration under 650 nm light irradiation. Additionally, the epidermal layer of mice appeared regular, and the thickness of the epidermis was more similar to normal skin compared with other groups. During the wound healing process, fibroblasts were widely distributed in dermal tissues and secreted collagen-rich extracellular matrix to support angiogenesis, granulation tissue formation and re-epithelialization.[39–41] Masson staining micro-scale examination indicated that new collagen deposition occurred in the regenerated skin tissue in all experimental groups throughout the wound-healing process (Fig. 7B). Under light irradiation, the newly formed blue collagen in the wounds treated with the antibacterial PCTL group was more apparent compared with the other groups, which was ascribed to the synergy between photodynamic therapy of the porphyrin part and chemotherapy of the quaternary ammonium salt group of the PCT membranes.

Angiogenesis is the key process during wound healing.[39] CD31 is an endothelial cell marker that could reflect the formation of new capillaries.[38–40] We analyzed the expression of CD31 in wound tissues by immunofluorescence histochemistry. As is shown in Fig. 8A and D, on the 7th day, wounds treated with the drug dressing showed higher expression of CD31-positive cells compared with naked wound tissues; in particular, the wounds in the PCTL group treated with PCT 0.5% antibacterial nanofiber membranes under 650 nm light irradiation exhibited a significantly higher number of CD31-positive cells compared with other groups. Macrophages affect wound repair by changing their phenotype. In the late stages of wound healing, macrophages polarize into M2 type and decrease the release of pro-inflammatory factors such as TNF-α, which is conducive to the removal of pathogens, apoptosis and necrotic tissue.[38–40] Thus, we detected the macrophage by the classical marker F4/80 (Fig. 8B and E) and the production of the TNF-α (Fig. 8C and F) in the wound tissues by immunofluorescence histochemistry and immunohistochemistry, respectively. Experimental results showed that more macrophage infiltration and significantly decreased production of TNF-α was observed in the PCTL group, and to a lesser extent also in the PCT group. These data show that compared with the blank group, PC group and commercially available 3 M materials, the PCT group (without light) also has a certain antibacterial repair effect, which proves our proposed antibacterial activity of quaternary ammonium salt groups. Further, the PCTL group can generate singlet oxygen by light which, combined with quaternary ammonium salts, achieve dual photodynamic and chemotherapeutic sterilization effects, thus accelerating angiogenesis and inhibiting advanced inflammation to promote the wound healing process. To conclude, the data in Fig. 8 suggests that PCTL treatment can promote the wound-healing process by accelerating angiogenesis and inhibiting the inflammation in late stage.

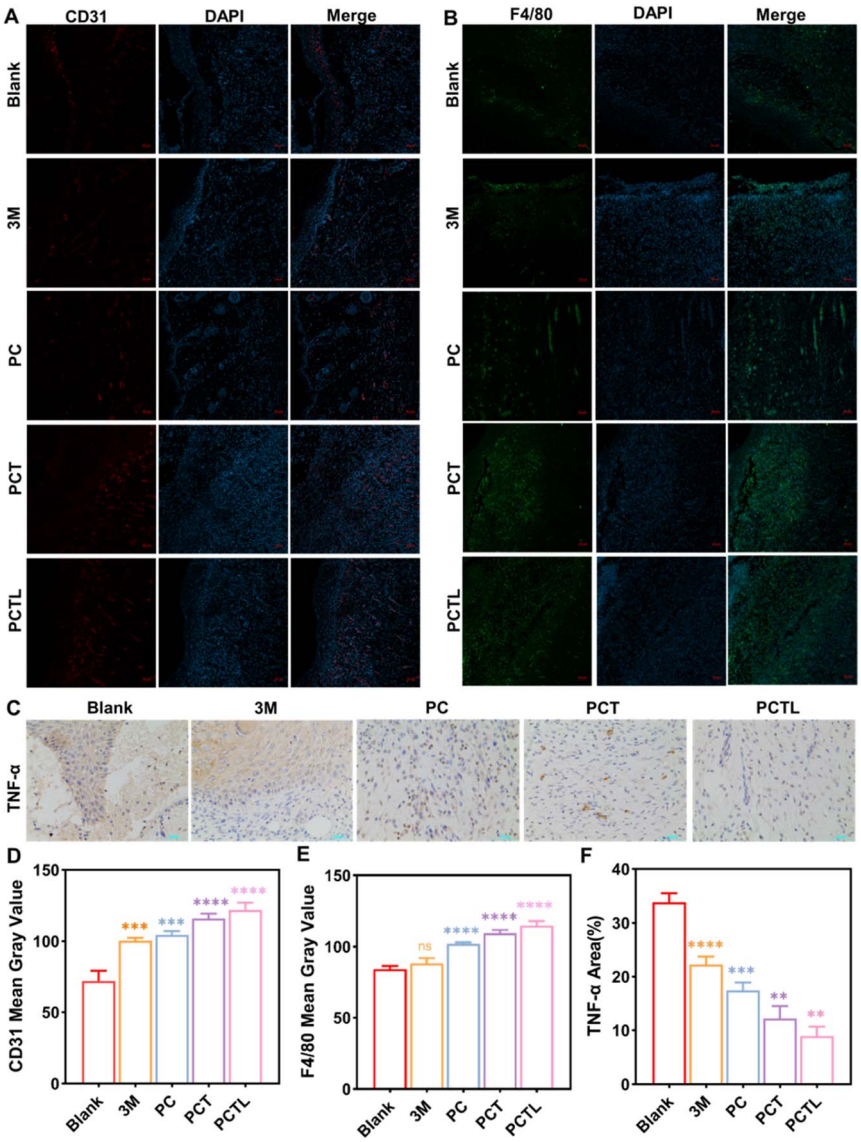


Fig. 8 Investigation of changes in angiogenesis and cytokines after treatment. (A) The expression of CD31 immunofluorescence in the skin wound of each group on day 7. (B) The expression of F4/80 immunofluorescence in the skin wound of each group on day 7. (C) Representative images of THF-α immunohistochemical staining on day 7. (D) CD31 mean gray value in the skin wound of each group on day 7 ($n = 4$). (E) F4/80 mean gray value in the skin wound of each group on day 7 ($n = 4$). (F) TNF-α area ratio in the skin wound of each group on day 7 ($n = 4$). $^{**}p < 0.01$, $^{***}p < 0.001$ and $^{****}p < 0.0001$.

## Experimental section

### Synthesis of 5-(4-hydroxyphenyl)-10,15,20-trimesitylporphyrin, TMP-OH

The synthesis method was based on existing literature.[28] A mixture of 1388 μL pyrrole, 2213 μL trimethylbenzaldehyde, 818.8 mg hydroxybenzaldehyde and 864 μL boron trifluoride ether was added to 1000 mL trichloromethane, stirred for one hour, then 3688.0 mg tetrachloro-1,4-benzoquinone was added. The product was cooled to room temperature and then distilled under reduced pressure until a dry solid was obtained. Purification was conducted through silica gel column chromatography using dichloromethane (DCM) as solvent. The first purple fraction was *meso*-tetrakis(4-methoxyphenyl)porphyrin (TMP), while the second purple fraction was TMPOH with a yield of 16%. $^1$H NMR (600 MHz, $CDCl_3$) $\delta$(ppm) in Fig. S1:† 8.83 (d, 2H, $J = 4.5$ Hz, pyrrole *H*), 8.71 (d, 2H, $J = 4.6$ Hz, pyrrole *H*), 8.67 (s, 4H, pyrrole *H*), 8.04 (d, 2H, $J = 8.3$ Hz, phenyl *H*), 7.30 (s, 6H, phenyl *H*), 7.10 (d, 2H, $J = 8.3$ Hz, phenyl *H*), 5.32 (s, 1H, phenyl-O*H*), 2.65 (d, 9H, $J = 4.0$ Hz, *p*-$CH_3$), 1.89 (s, 18H, *o*-$CH_3$), −2.51 (br, s, 2H, α-pyrrole-N*H*). $^{13}$C NMR (DEPT, 151 MHz, $CDCl_3$) $\delta$(ppm) in Fig. S2:† 135.44 (s, porphyrin carbon), 127.88 (s, porphyrin carbon), 113.54 (s, porphyrin carbon), 21.63 (d, –$CH_3$), 21.41(s, –$CH_3$). ESI-MS *m*/*z* calcd for $C_{53}H_{49}N_4O$ in Fig. S3,† $[M + H]^+$, 757.3902; found: 757.3901.

### Synthesis of 5-[4-(6-bromo-1-hexoxy) phenyl]-10,15,20-trimesitylporphyrin, TMP-O$(CH_2)_6$Br

TMP-OH (300.0 mg, 0.40 mmol) was dissolved in 10 mL of acetone, and then mixed with NaOH (293.4 mg, 7 mmol) before

stirring for 4–8 h. After adding 1 mL of 1,6-dibromohexane, the mixture was heated at 65 °C. The reaction process was monitored by TLC and was stopped after 20 h. At the end of the reaction, the purple solids obtained by vacuum distillation were washed with petroleum ether (PE) to remove excess 1,6-dibromohexane. The collected purple solid was separated by silica gel column chromatography with DCM/PE (1 : 3) as the eluent, and the first purple component TMP-O$(CH_2)_6$Br was collected in a 70% yield. $^1$H NMR (600 MHz, $CDCl_3$) $\delta$(ppm) in Fig. S4:† 8.83 (d, 2H, $J = 4.5$ Hz, pyrrole *H*), 8.69 (d, 2H, $J = 4.6$ Hz, pyrrole *H*), 8.64 (s, 4H, pyrrole *H*), 8.11 (d, 2H, $J = 8.4$ Hz, phenyl *H*), 7.28 (d, 8H, $J = 8.8$ Hz, phenyl *H*), 4.27 (t, 2H, $J = 6.4$ Hz, –O$CH_2$–), 3.75 (t, 2H, $J = 6.5$ Hz, –C$H_2$Br), 2.64 (d, 9H, $J = 4.1$ Hz, *p*-C$H_3$), 2.01 (d, 2H, $J = 14.3$ Hz, –O$CH_2CH_2CH_2CH_2CH_2CH_2$Br), 1.87 (d, 18H, $J = 4.3$ Hz, *o*-C$H_3$), 1.71 (s, 4H, –O$CH_2CH_2CH_2CH_2CH_2CH_2$Br), 1.59 (s, 2H, –O$CH_2CH_2CH_2CH_2CH_2CH_2$Br), −2.52 (br, s, 2H, α-pyrrole-N*H*). $^{13}$C NMR (DEPT, 151 MHz, $CDCl_3$) $\delta$(ppm) in Fig. S5:† 135.37 (s, porphyrin carbon), 127.67 (s, porphyrin carbon), 112.6 (s, porphyrin carbon), 67.97 (s, phenyl-O$CH_2$–), 33.83 (s, –O$CH_2CH_2CH_2CH_2CH_2$Br), 32.6 (s, –O$CH_2CH_2CH_2CH_2CH_2CH_2$Br), 29.29 (s, –O$CH_2CH_2CH_2CH_2CH_2CH_2$Br), 28.02 (s, –O$CH_2CH_2CH_2CH_2CH_2CH_2$Br), 25.46 (s, –O$CHs_2CH_2CH_2CH_2CH_2CH_2$Br), 21.63(d, –C$H_3$), 21.42 (s, –C$H_3$). ESI-MS *m*/*z* calcd for $C_{59}H_{60}BrN_4O$ in Fig. S6,† $[M + H]^+$, 919.3945; found: 919.3947.

### Synthesis of *N*,*N*-bis-(2-hydroxyethyl)-*N*-(6-(4-(10,15,20-trimesitylporphyrin-5-yl) phenoxy) hexan)-*N*-methanaminium bromide, TMP-O$(CH_2)_6$N+$(C_2H_4OH)_2CH_3$Br–, TMP(+)

A dimethylformamide (DMF) (1 mL) solution of TMPO$(CH_2)_6$Br (100.0 mg, 0.11 mmol) was added to 1 mL of *N*-methyldiethanolamine, heated at 80 °C for 20 h. The solvent DMF was removed and 30 mL distilled water was added to wash the solid repeatedly. After drying in the oven, the final yield of the purple solid $TMP^{(+)}$ was 87%. $^1$H NMR (600 MHz, $d_6$-DMSO) $\delta$(ppm) in Fig. S7:† 8.79–8.42 (m, 8H, pyrrole *H*), 8.03 (s, 2H, phenyl *H*), 7.26 (s, 8H, phenyl *H*), 5.25 (s, 2H, –O*H*), 4.18 (s, 2H, –O$CH_2$–), 3.80 (s, 4H, –C$H_2$OH), 3.42 (s, 6H, –NC$H_2$–), 3.06 (s, 3H, –NC$H_3$), 2.43 (s, 9H, *p*-C$H_3$), 1.69 (s, 27H, –C$H_3$, –O$CH_2CH_2CH_2CH_2CH_2CH_2$N–), −2.75 (br, s, 2H, α-pyrrole-N*H*). $^{13}$C NMR (DEPT, 151 MHz, $d_6$-DMSO) $\delta$ (ppm) in Fig. S8:† 135.03 (s, porphyrin carbon), 127.61(s, porphyrin carbon), 112.63 (s, porphyrin carbon), 67.33 (s, –O$CH_2CH_2CH_2CH_2CH_2CH_2$N–), 63.03 (s, –*N*–$CH_2CH_2$OH), 62.19 (s, –O$CH_2CH_2CH_2CH_2CH_2CH_2$N–), 54.59(s, –*N*–$CH_2CH_2$OH), 48.82 (s, –*N*–C$H_3$), 28.42 (s, –O$CH_2CH_2CH_2CH_2CH_2CH_2$N–), 25.41 (s, –O$CH_2CH_2CH_2CH_2CH_2CH_2$N–), 24.99 (s, –O$CH_2CH_2CH_2CH_2CH_2CH_2$N–), 21.38 (s, –O$CH_2CH_2CH_2CH_2CH_2CH_2$N), 21.07 (s, –C$H_3$), 20.95 (s, –C$H_3$), 20.78 (s, –C$H_3$). ESI-MS *m*/*z* calcd for $C_{64}H_{72}N_5O_3$ in Fig. S9,† $[M–Br^-]^+$, 958.5629, found: 958.5638.

### Preparation of PC, PCT and PCP nanofiber membranes

360.0 mg PCL and 240.0 mg COL were dissolved in 10 mL of hexafluoroisopropanol and then stirred magnetically for 12 h at room temperature until the solution became homogeneous. $TMP^{(+)}$ with a mass of 0 mg, 2.0 mg, 5.0 mg, 10.0 mg, 20.0 mg, 50.0 mg and TMPOH with a mass of 50 mg were weighed and dissolved in 10 mL of the PCL/COL homogeneous solution. Then, the solution was electrospun using an electrospinning machine (YFSP-T, Tianjin Yunfan Instrument CO. Ltd, China). The spinning parameters were set as: the syringe, 10 mL; the voltage, 16 kV; the flow rate, 1.0 mL $h^{-1}$; the acceptance distance, 18 cm; environmental temperature, 28.0 ± 3.0 °C, and humidity, 40.0 ± 10.0%. The resulting nanofiber membranes are hereafter referred to as PC, PCT 0.02%, PCT 0.05%, PCT 0.1%, PCT 0.2%, PCT 0.5% and PCP 0.5%, respectively, depending on the amount of porphyrin used. The PC, PCT and PCP nanofiber membranes were vacuum-dried at room temperature for three days to remove the residual solvent.

### SEM test

The surface of PC and PCT nanofiber membranes were sprayed with gold and photographed by SEM (EVO LS15, Zeiss, Germany) to observe the surface fiber morphology, pore distribution and other morphological characteristics. One hundred fibers were randomly selected for diameter distribution statistics by Image J (National Institutes of Health, USA).

### Contact angle test

The contact angles of the PC and PCT nanofiber membranes were measured by a contact angle meter (SZ-CAMD33, China) based on the standard solid drop method. The nanofiber membrane was laid flat on a slide and 1 μL of distilled water was dropped onto it. When the water drop touched the fiber membrane, the contact angle image was taken using a high-speed camera. The contact angle was statistically averaged over 8 trials.

### TGA determination

The thermogravimetric analysis (TGA) curves of the PC and PCT nanofiber membranes were recorded on a thermal analyzer (DSC 3+/1100LF, METTLER TOLEDO, Switzerland). The samples (about 7.5 mg) were placed in the sample holder for testing with the parameters as nitrogen flow rate, 40 mL $min^{-1}$; heating range, 25–500 °C; heating rate, 10 °C $min^{-1}$; cooling rate, 20 °C $min^{-1}$.

### ROS detection

The absorbance of DPBF at 410 nm is irreversibly quenched by $^1O_2$,[30] and can be used as a chemical sensing probe to measure the ROS production by PC, PCT (PCT 0.02%, PCT 0.05%, PCT 0.1%, PCT 0.2% and PCT 0.5%) and PCP 0.5% nanofiber membranes under light irradiation. A methanol solution containing DPBF (14 μg $mL^{-1}$) and a PCT nanofiber membrane (1.0 × 1.0 $cm^2$) was continuously irradiated with a 9.0 ± 0.5 mW $cm^{-2}$ lamp panel (12.0 × 10.0 $cm^2$) with 650 ± 10 nm LEDs (KTG, JIADENG, China) for 80 min. Then the absorbance at 410 nm was recorded by an ultraviolet-visible spectrometer (DS-11 FX+, DeNovix, USA) with the control group.

### Cycle experiment

A 15 mL (14 μg $mL^{-1}$) DPBF solution was prepared, its initial absorbance under dark conditions was measured, and the

solution was stored in the dark. The PCT nanofiber membrane ($1.0 \times 1.0$ cm$^2$) with a concentration of 0.5% TMP$^{(+)}$ (PCT 0.5%) was unfolded in 1 mL of the aforementioned DPBF solution. The absorbance at the beginning of the first cycle was measured with a UV-visible photometer (DS-11 FX+, DeNovix, USA). Then, the solution was illuminated for 30 min ($9.0 \pm 0.5$ mW cm$^{-2}$, $650 \pm 10$ nm), and the absorbance after the illumination was measured. After the test, the PCT 0.5% nanofiber membrane ($1.0 \times 1.0$ cm$^2$) was taken out and another 1 mL of the above solution was added again, and the absorbance was again measured after 30 min of 650 nm light irradiation. The cycle was repeated 10 times.

### Cytotoxicity test

The cytotoxicity assay was performed using mouse fibroblasts (L929) as experimental cells, which were evaluated by the CCK-8 assay.[29] Sterilized PC and PCT (PCT 0.02%, PCT 0.05%, PCT 0.1%, PCT 0.2% and PCT 0.5%) nanofiber membranes ($1.0 \times 1.0$ cm$^2$) were placed on the bottom of 24-well plates. L929 cells were seeded onto the PC and PCT membrane at a density of $5 \times 10^4$ cells per well. After 24 hours of incubation in a humidified environment containing 5% carbon dioxide, the 24-well plates were removed from the incubator and placed under light ($9.0 \pm 0.5$ mW cm$^{-2}$, $650 \pm 10$ nm). Parallel experiments without fiber membranes were used as a control. After 3 hours of illumination, the medium was removed and incubated with CCK-8 solution. At the end of the incubation, the supernatant was taken and the OD value at 450 nm was measured using a microplate reader. The result was recorded as the OD value relative to the control under dark conditions.

### Antibacterial test

G$^+$ *S. aureus* and G$^-$ *E. coli* were selected as experimental strains to evaluate their antibacterial activity. The experimental PC and PCT (PCT 0.02%, PCT 0.05%, PCT 0.1%, PCT 0.2% and PCT 0.5%) nanofiber membranes ($1.0 \times 1.0$ cm$^2$) were disinfected and spread on the bottom of the 24-well plate. After adding 100 μL ($10^6$ CFU mL$^{-1}$) of the bacterial suspension to each well, the membranes were incubated in 37 °C darkness for 5 hours and then illuminated for 3 hours ($9.0 \pm 0.5$ mW cm$^{-2}$, $650 \pm 10$ nm). Subsequently, 900 μL sterile Phosphate Buffered Saline (PBS) was added and the bacteria on the membrane surface were moved by ultrasound (3 min). Subsequently, 100 μL of diluted G$^+$ *S. aureus* and G$^-$ *E. coli* suspensions were placed on sterile LB AGAR plates and incubated overnight at 37 °C to obtain visible colonies. The number of colonies on each plate was then counted to estimate the total number of live bacteria adhering to each sample. Each experiment was performed three times, and the distribution of bacteria on the membrane was observed with scanning electron microscopy.

### Hemolysis rate test

The hemocompatibility of the dressing was tested using red blood cells (RBCs) from Balb/c mice (19–21 g, 8 weeks).[41] After ultraviolet (UV) sterilization, the PC and PCT (PCT 0.02%, PCT 0.05%, PCT 0.1%, PCT 0.2% and PCT 0.5%) nanofiber membranes were cut to $1.0 \times 1.0$ cm$^2$, then placed at the bottom of a 24-well culture plate. The eyeballs of Balb/c mice were bled, then 1 mL of blood taken from the mice was centrifuged to separate the supernatant from the red blood cells. The RBCs were then washed twice, re-suspended, and diluted with 30 mL of PBS (10 mM, pH = 7.2–7.4). Thereafter, 1 mL of the diluted red blood cells was added onto the nano-dressing of the 24-well culture plate, then incubated at 37 °C for 1 h. The extracts from each well were collected and centrifuged at 1000 rpm for 10 min to separate the supernatant. The absorbance of the separated supernatant was measured at 540 nm using a microplate reader. Triton X-100 (0.1%) to red blood cells was used as a positive control ($n = 4$, for all groups), and 0.1% PBS was added to red blood cells as a blank control.

### *In vivo* test

All animal experiments were approved by the Institutional Animal Care Committee. To better acclimate to the experiment, the 72 Balb/c mice (19–21 g, 8 weeks) were raised under standard conditions ($24.0 \pm 2.0$ °C) over 7 days in an animal room. The mice were randomly divided into 5 groups (12 mice in each group): the blank group (untreated group), 3 M group (positive drug controlled group, Tegaderm Film dressing), the PC group (POL/COL without TMP$^{(+)}$), the PCT group (PCT 0.5% membrane, without light) and the PCTL group (PCT 0.5% membrane, with $9.0 \pm 0.5$ mW cm$^{-2}$, $650 \pm 10$ nm light treatment on the 1st day and 3rd day for 3 h each time). The mice were anesthetized through intraperitoneal injection of 7% chloral hydrate (0.6 mL/100 g), then a full-thickness wound (about 8 mm in diameter) was created on the dorsal skin of each mouse. Afterward, 20 μL of G$^+$ *S. aureus* suspension ($10^8$ CFU mL$^{-1}$) was inoculated into the wound and maintained for 18 h to establish an infection model. Treatment after infection involved one of the following strategies: the experimental (PC, PCT 0.5%, PCTL) and control (3 M) groups were covered with dressing on the wound, and the blank group (blank) was not treated. For wound healing data collection, mice were sacrificed on the 3rd, 7th, and 14th days following surgery. Fixation, embedding, and cross-sectioning of tissue samples were performed. Angiogenesis, inflammatory cell infiltration, and fibroblast proliferation were assessed with hematoxylin–eosin (H&E) staining, and collagen deposition was observed with Masson's trichrome staining.[38,39]

### Immunohistochemistry and immunofluorescence assays

We performed immunohistochemistry and immunofluorescence assays as described earlier.[38–40] Embedded mouse wound tissue on day 7 cuts was cut into 5 mm slices with a rotatory microtome (RM2245, Leica Microsystems, Germany) and incubated overnight at 4 °C with corresponding primary antibodies. For the immunohistochemistry assay, wound tissue slices were incubated with horseradish peroxidase-labeled secondary antibody and stained with diaminobenzidine. The samples were scanned under a light microscope (DM1000, Leica, Germany). As part of the immunofluorescent assay, tissue slices were incubated with fluorescent-labeled secondary antibodies and 4′,6-diamidino-2-phenylindole (DAPI) for nuclei staining. The samples were imaged by laser scanning confocal microscopy

(LSM800, Zeiss, Germany). Quantitative analysis was performed by Image J (National Institutes of Health, USA).

### Statistical analysis

A statistical analysis of the data was performed using GraphPad Prism 8. All data are expressed as mean ± SD (standard deviation). Statistical analysis was performed using analysis of variance (ANOVA) and $P < 0.05$ was considered statistically significant (* for $P < 0.05$, ** for $P < 0.01$, *** for $P < 0.001$, and **** for $P < 0.0001$ and NS = no significance).

## Conclusions

In this study, we designed and synthesized a molecule with a dual antibacterial function, $TMP^{(+)}$, that displays chemotherapy and photodynamic therapy activities simultaneously. The porphyrin part of the $TMP^{(+)}$ molecule can produce singlet oxygen for photodynamic sterilization, which enhances the therapeutic effect and reduces the required concentration of the cytotoxic quaternary ammonium salt antibacterial agents. Moreover, the introduction of positive charge centers is beneficial for countering the self-quenching effect caused by π–π interaction of the planar large conjugate porphyrin ring, thereby improving the efficiency of singlet oxygen production.[19–23] Last but not least, the cationic porphyrin molecule $TMP^{(+)}$ can bind to negative charges on the surface of bacteria to improve targeting and thus enhance the therapeutic effects.[26–28,31–33] *In vitro* antibacterial experiments fully proved that the antibacterial efficiency could be enhanced under illumination (660 nm, 9 mW $cm^{-2}$), due to the opening up of the photodynamic therapy pathway. Based on these results, we used a novel $TMP^{(+)}$ molecule to design and construct a new nanofiber dressing PCT, with photodynamic and chemical antibacterial properties that efficiently promote wound healing in $G^+$ *S. aureus* infections. PCT was prepared by blending PCL, COL and $TMP^{(+)}$ using electrospinning technology. The results show that PCT dressing has good biocompatibility and antibacterial effect in the dark, the latter of which could be enhanced with light. PCT dressings (either with or without light) also promoted cell proliferation, tissue granulation and collagen deposition under light conditions. The expression experiments of related cytokines (CD31, F4/80, TNF-α) further confirmed the photo-bactericidal activity of the PCT dressing. In conclusion, PCT is expected to become an effective dressing for the healing of infected wounds, providing a reference for the application of PDT therapy in the biomedical field.

## Institutional review board statement

The animal study protocol was approved by the Biomedical Research Ethics Committee of Binzhou Medical University (Ethics Section 2023 No. 205).

## Data availability

Data described in the manuscript are available from the corresponding author on reasonable request.

## Author contributions

J. Zhang, L. Ma and L. Chen designed the research and wrote the final paper. X. Yuan was in charge of data curation and the first draft. X. Yuan, J. Zhang and Y. Zhang explored and designed experiments. H. Li, K. Pang, C. Sun, J. Li and Z. Liu synthesized and characterized porphyrin derivatives. X. Yuan and L. Yu made the mechanism charts and accomplished the discussions related to the biological effects. L. Chen, J. Song and L. Ma provided the scientific direction and resource related to the biological and chemical experiments.

## Conflicts of interest

There are no conflicts to declare.

## Acknowledgements

This research was funded by the National Natural Science Foundation of China (No. 22001020), Foundation of Binzhou Medical University (No. 2019KYQD23, 2022KYQD27). We are grateful for the Yantai Double Hundred Plan and Yantai Medical Antibacterial Material Innovation Service Platform. We thank Dr Zikuan Wang (Max-Planck-Institut für Kohlenforschung) and Mr Chaoyang Zhang (Shandong University of Traditional Chinese Medicine) for graphic and textual proofreading of the manuscript.

## Notes and references

1 E. D. Brown and G. D. Wright, *Nature*, 2016, **529**, 336.
2 World Health Organization, *Global Guidelines on the Prevention of Surgical Site Infection*, 2022.
3 Y. Liu, H. J. Busscher, B. Zhao, Y. Li, Z. Zhang, H. C. v. d. Mei, Y. Ren and L. Shi, *ACS Nano*, 2016, **10**, 4779.
4 X. Dai, Q. Guo, Y. Zhao, P. Zhang, T. Zhang, X. Zhang and C. Li, *ACS Appl. Mater. Interfaces*, 2016, **8**, 25798.
5 W. C. Huang, R. Ying, W. Wang, Y. N. Guo, Y. J. He, X. Y. Mo, C. H. Xue and X. Z. Mao, *Adv. Funct. Mater.*, 2020, **30**, 2000644.
6 W. Zhan, Y. Qu, T. Wei, C. Hu, Y. Pan, Q. Yu and H. Chen, *ACS Appl. Mater. Interfaces*, 2018, **10**, 10647.
7 H. Xu, Z. Fang, W. Tian, Y. Wang, Q. Ye, L. Zhang and J. Cai, *Adv. Mater.*, 2018, **30**, 1801100.
8 Y. Liang, Y. Liang, H. Zhang and B. Guo, *Asian J. Pharm. Sci.*, 2022, **17**, 353.
9 X. P. Feng, B. Tong, J. B. Shi, Z. X Cai, C. S. Zhao and Y. P Dong, *Mater. Chem. Front.*, 2021, **5**, 1164.
10 E. Polat and K. Kang, *Biomedicines*, 2021, **9**, 30.
11 J. L. Kan, Y. Jiang, A. Xue, Y. H. Yu, Q. Wang, Y. Zhou and Y. B. Dong, *Inorg. Chem.*, 2018, **57**, 5420.
12 D. E. Dolmans, D. Fukumura and R. K. Jain, *Nat. Rev. Cancer*, 2003, **3**, 380.
13 T. C. Pham, V. N. Nguyen, Y. Choi, S. Lee and J. Yoon, *Chem. Rev.*, 2021, **121**, 13454.
14 T. Zhang, Y. Deng, S. L. Chua, B. Z. Tang and B. L. Khoo, *Chem. Eng. J.*, 2022, **447**, 137579.

15 S. Gnanasekar, G. Kasi, X. He, K. Zhang, L. Xu and E. T. Kang, *Bioact. Mater.*, 2023, **21**, 157.
16 E. Pang, S. Zhao, B. Wang, G. Niu, X. Song and M. Lan, *Coord. Chem. Rev.*, 2022, **472**, 214780.
17 H. Abrahamse and M. R. Hamblin, *Biochem. J.*, 2016, **473**, 347.
18 A. F. Espitia, M. R. Valle, Q. E. Navarro, L. L. C. Pacheco and F. N. J. Galán, *Pharmaceuticals*, 2023, **16**, 1059.
19 P. Ran, T. Xia, H. Zheng, F. Lei, Z. Zhang, J. Wei and X. Li, *Acta Biomater.*, 2023, **155**, 292.
20 L. C. Makola, M. Managa and T. Nyokong, *Photodiagnosis Photodyn. Ther.*, 2020, **30**, 101736.
21 Y. Zhao, M. Yuan, H. Yang, J. Li, Y. Ying, J. Li, W. Wang and S. Wang, *Small*, 2023, e2305189.
22 B. X. Xie, H. S. Wang, H. Q. Zheng, J. Xu, L. Chen, F. Z. Zhang, Y. L. Wang, Z. J. Lin and R. G. Lin, *Inorg. Chem.*, 2023, **62**, 13892.
23 J. F. Lovell, C. S. Jin, E. Huynh, H. Jin, C. Kim, J. L. Rubinstein, W. C. W. Chan, W. Cao, L. V. Wang and G. Zheng, *Nat. Mater.*, 2011, **10**, 324.
24 C. S. Jin, J. F. Lovell, J. Chen and G. Zheng, *ACS Nano*, 2013, **7**, 2541.
25 J. Chen, Y. Zhu and S. Kaskel, *Angew. Chem., Int. Ed.*, 2021, **60**, 5010.
26 Y. X. Zhu, H. R. Jia, Z. Chen and F. G. Wu, *Nanoscale*, 2017, **9**, 12874.
27 Y. Jiao, L. N. Niu, S. Ma, J. Li, F. R. Tay and J. H. Chen, *Prog. Polym. Sci.*, 2017, **71**, 53.
28 W. Cui, X. P. Zhang and B. B. Wayland, *J. Am. Chem. Soc.*, 2003, **125**, 4994.
29 Y. Mi, Y. Chen, G. Gu, Q. Miao, W. Tan, Q. Li and Z. Guo, *Carbohydr. Polym.*, 2021, **273**, 118623.
30 R. H. Alshammari, U. C. Rajesh, D. G. Morgan and J. M. Zaleski, *ACS Appl. Bio Mater.*, 2020, **3**, 7631.
31 H. Taslı, A. Akbıyık, N. Topaloğlu, V. Alptüzün and S. Parlar, *J. Microbiol.*, 2018, **56**, 828.
32 M. R. Detty, S. L. Gibson and S. J. Wagner, *J. Med. Chem.*, 2004, **47**, 3897.
33 V. M. Lechner, M. Nappi, P. J. Deneny, S. Folliet, J. C. K. Chu and M. J. Gaunt, *Chem. Rev.*, 2022, **122**, 1752.
34 X. Feng, J. Lei, L. Ma, Q. Ouyang, Y. Zeng, H. Liang, C. Lei, G. Li, L. Tan, X. Liu and C. Yang, *Small*, 2022, **18**, e2105775.
35 W. Dong, Z. Li, W. Wen, B. Liu and G. Wen, *ACS Appl. Mater. Interfaces*, 2021, **13**, 57497.
36 J. Li, L. Qu, H. Li, L. Zhao, T. Chen, J. Liu, Y. Gao and H. Pan, *Mikrochim. Acta*, 2023, **190**, 366.
37 Z. Wang, F. J. Xu and B. Yu, *Front. Bioeng. Biotechnol.*, 2021, **9**, 783354.
38 Y. Wang, D. Xiao, H. Yu, Y. Zhong, L. Zhang, X. Sui, B. Wang, X. Feng, H. Xu and Z. Mao, *Int. J. Biol. Macromol.*, 2023, **224**, 1382.
39 A. D. J. Bombin, N. Dunne and H. O. McCarthy, *Acta Biomater.*, 2023, **155**, 304.
40 Y. Wang, M. Yang and Z. Zhao, *Carbohydr. Polym.*, 2023, **310**, 120723.
41 Q. Cheng, Z. Wang, S. Hu, Y. Y. Peng, R. Zhu, L. Zhang, J. Li and R. Narain, *J. Mater. Chem. B*, 2023, **11**, 7228.
42 Z. Zheng, X. Yang, M. Fang, J. Tian, S. Zhang, L. Lu, C. Zhou, C. Xu, Y. Qi and L. Li, *Regener. Biomater.*, 2023, **10**, 72.